Published by IOP Publishing for Sissa Medialab

Received: *June 28, 2019*
Revised: *October 25, 2019*
Accepted: *December 9, 2019*
Published: *January 23, 2020*

3rd European Conference on Plasma Diagnostics (ECPD2019)
6–10 May 2019
Lisbon, Portugal

Benchmarking of the EM modelling of the ITER plasma position reflectometry in-vessel antennas with a metallic target using prototype tests

J.H. Belo,[1] P. Varela and A. Silva

Instituto de Plasmas e Fusão Nuclear, Instituto Superior Técnico, Universidade de Lisboa, Av. Rovisco Pais 1, 1049-001 Lisboa, Portugal

E-mail: jbelo@ipfn.tecnico.ulisboa.pt

Abstract: Studies have shown the importance of modelling the main surfaces of the narrow openings between blanket modules (BMs) through which the antennas of the ITER Plasma Position Reflectometry (PPR) systems located inside the vacuum vessel probe the plasma. This is especially important for the system located in the high-field side (gap 6), where the cut-outs in the surfaces of BMs strongly shape the antenna's radiation pattern, notably at lower frequencies. In addition, the (slanted) geometry of the first-wall (FW) panels may hinder the performance of the system by focusing the multiple reflections between the plasma and the FW back to the antenna. For the system located in the low-field side (gap 4), the opening between the BMs decreases towards the plasma, which together with the step in the top BM behind the antennas and the slanted arrangement of the FW panels also imposes challenges to the performance of the system. Comparisons of 3D electromagnetic (EM) simulations to laboratory tests of the antenna prototype, including mock-ups of the BMs as well as a metallic target, aiming to benchmark the simulations, reveal good agreement.

Keywords: Microwave Antennas; Nuclear instruments and methods for hot plasma diagnostics

[1]Corresponding author.

https://doi.org/10.1088/1748-0221/15/01/C01033

Contents

1 **Introduction** 1

2 **Benchmarking of gap 6 results** 3

3 **Benchmarking of gap 4 results** 4

4 **Conclusions** 5

2020 JINST 15 C01033

1 Introduction

The ITER Plasma Position Reflectometry (PPR) diagnostic consists of four O-mode reflectometers to measure the edge density profile at four locations, known as gaps 3, 4, 5 and 6, for plasma position control purposes, particularly during long discharges [1]. In gaps 4 and 6 the antennas are installed in-vessel and consist of bistatic arrays of parallel 115 mm long pyramidal horns, one for emission, one for reception. The antennas operate in the frequency range 15 GHz to 75 GHz and are fed by rectangular waveguides (internal section of 20 mm × 12 mm and set 9.5 mm apart) with the TE_{01} mode (E-field along the larger dimension). For gap 6 (figure 1, top) the antennas are installed in the high-field side, close to the equatorial plane, between blanket modules (BMs) #3 and #4. In gap 4 (figure 1, bottom) the antennas are in the low-field side, well above the equatorial plane, between BMs #11 and #12.

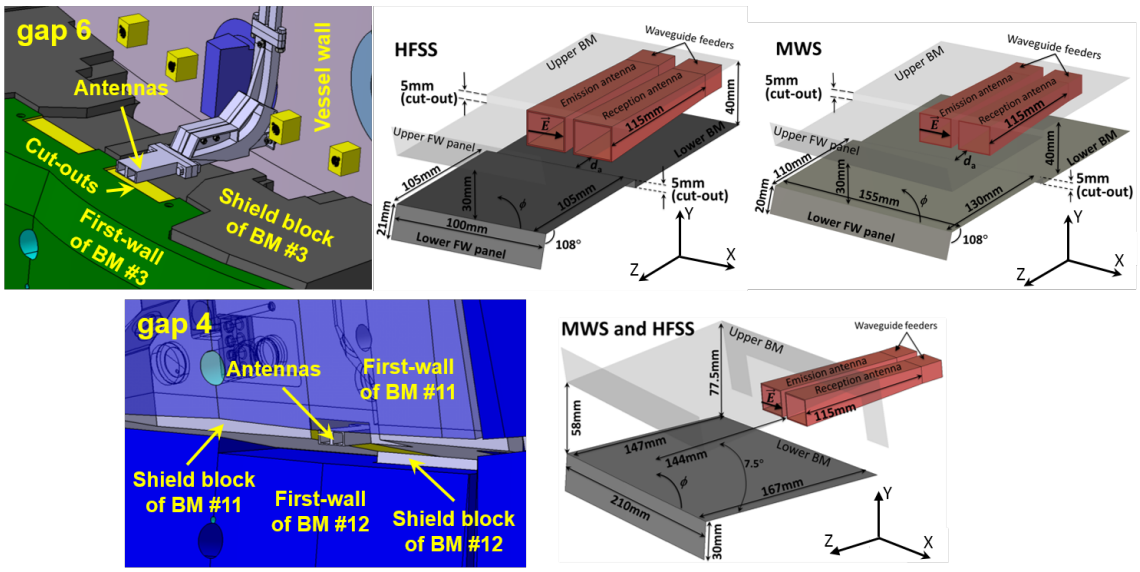

Figure 1. Top: CAD model of gap 6, with the top BM #4 removed for clarity (left), and EM models of HFSS (centre) and MWS (right). Bottom: CAD model of gap 4 (left) and EM model of HFSS and MWS (right).

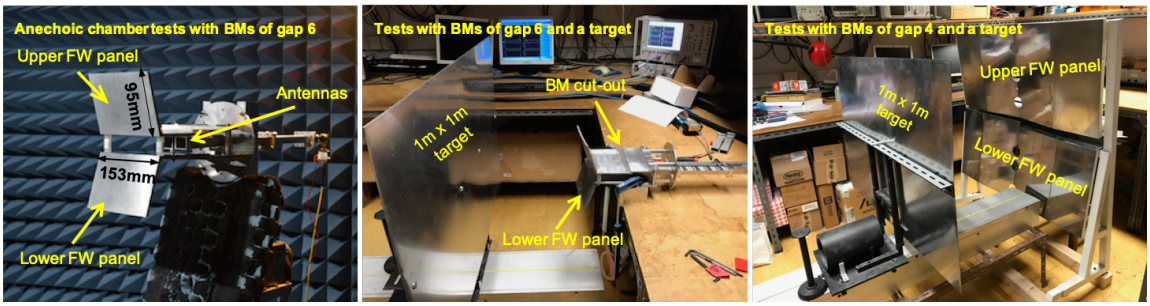

Figure 2. Measurement of the radiation patterns for gap 6 (left) and measurement of the coupling via the metallic target for gaps 6 (centre) and 4 (right).

Previous 3D electromagnetic simulation have shown [2] the impact of the narrow openings through which the antennas probe the plasma, which impose small low-gain antennas, thus low antenna-target coupling. For gap 6 the BM cut-outs cause unwanted strong reflections back to the antenna, notably at lower frequencies, while the slanted first-wall (FW) panels capture, back to the antennas, the multiple reflections between the plasma and the FW. For gap 4 the height of the opening decreases towards the plasma, which shatters the main lobe and creates multiple lines-of-sight. Moreover, the step in the top BM, behind the antennas, and the slanted FW compound to create unwanted reflections, multiple-mode field configurations and resonances.

Given these issues and taking into account that once installed in the ITER vacuum vessel these components are not maintainable for the lifetime of the machine, it was decided to prototype the antennas to assess the performance of the in-vessel systems before installation. Prior to prototyping, the design of the antennas was iterated and optimised in terms of reflection coefficient (S_{11}) and coupling (S_{21}), both direct and via the metallic target, using 3D electromagnetic (EM) simulations with Ansys HFSS and CST MWS, taking into account the effect of the surrounding BMs [2, 3]. The optimised antennas feature symmetric toroidal and poloidal flares of 2 mm and 4 mm, i.e. apertures of 24 mm × 20 mm and a distance between tips of 5.5 mm — the toroidal and poloidal directions run along the larger and smaller dimensions of the antennas, respectively. In the current design the antennas are located at a distance $d_a = 15$ mm from the BM cut-outs. However, the optimisation studies [2] have shown that the impact of the cut-outs can be mitigated by positioning the antennas at $d_a = 10$ mm. The results presented here pertain the latter configuration.

In the EM simulations, all elements were modelled as perfect electric conductors — the antennas and feeders using 3D components with 1 mm thick walls whereas the remaining elements were truncated and modelled using sheets (to reduce the computational burden) — and the feeders excited with the TE_{01} mode. HFSS used their flagship, but computationally heavy (frequency-domain) Modal solver, in which the solution is computed for discrete frequencies (here using a 0.1 GHz step). For MWS, although it provides a frequency-domain solver, the simulations were carried out using its much faster (time-domain) Transient solver, in which the solutions are obtained for the entire frequency range in a single run, allowing the test of more design variations and being also an opportunity to benchmark the results of two very different solvers. In the vicinity of the antennas the FW panels are slanted in the poloidal direction and curved in the toroidal direction (figure 1); in MWS both features were modelled using a (slanted) flat sheet, which is 130 mm from

2020 JINST 15 C01033

the cut-out in one end and 110 mm on the other end, whereas in the (former) HFSS simulations, a previous less faithful model was used, in which both ends of the (slanted) flat sheet are 105 mm from the cut-out. The symmetries of the model and E-field of the TE_{01} mode with respect to the XZ plane allowed for a magnetic symmetry boundary to be applied in MWS across this plane to reduce the computational load. In HFSS, no symmetries could be applied due to the schemes used to reduce the computational burden. Once manufactured, the prototype antennas were tested in an anechoic chamber. Their radiation patterns were determined with and without the mock-ups of the BMs. Then, reflection and coupling coefficients with and without BMs were measured using a metallic target emulating the plasma reflection layer, as shown in figure 2.

The benchmarking of the results obtained for gaps 6 and 4 with the simulation tools against the prototype tests is presented in sections 2 and 3. It regards the radiation pattern, reflection coefficient and coupling, both direct and via the metallic target. For cost reduction, the design of the PPR system uses the same antennas for both gaps. Due to the more stringent restrictions of gap 6, the design of the antennas was optimised for this gap (in terms of S_{11} and S_{21} [2, 3]).

2 Benchmarking of gap 6 results

Figure 3 depicts the radiation patterns obtained from HFSS, MWS and anechoic chamber tests without (top) and with (bottom) BMs, in the H-plane of the antennas (poloidal plane, $\phi = 90°$). Figure 3 and the following show also, unless stated otherwise, A_C^B, the percentage of the range over which the difference between MWS and HFSS is $< B$ for a threshold above noise C, here $B = 3\,\mathrm{dB}$ and $C = -20\,\mathrm{dB}$. They are remarkably similar without BMs, with $A_C^B > 90\%^{3dB}_{-20dB}$ for all frequencies, revealing the broad radiation patterns in the lower frequencies due to the reduced poloidal flare and the E-field orientation of the TE_{01} mode. With BMs the differences between the solvers and, most notably, between the BM models used in MWS and HFSS show up (cf. figure 6) in the differences in the level of the main lobe — as in the E-plane (toroidal plane, $\phi = 0°$) results (not shown) — and $54\%^{3dB}_{-20dB} < A_C^B < 82\%^{3dB}_{-20dB}$. Still, both HFSS and MWS reveal the strong impact of the BMs in agreement with the experimental results: the larger directivity of the radiating structure formed by the antennas, BMs and FW panels, into which the antenna radiates, narrows the beam inducing a focusing effect; and the reflections from the BM cut-outs create side- and back-lobes. This is more significant at lower frequencies, due to the broader antenna beam, while for higher frequencies high-amplitude secondary lobes appear close to the main lobe — in the E-plane (not shown) the BM aperture is sufficiently large and does not affect significantly the radiation patterns.

The results for the reflection coefficient (S_{11}) and direct coupling (S_{21}) obtained from HFSS and MWS, with and without BMs, are depicted in figure 4 (with $C = -60\,\mathrm{dB}$), where the overall agreement between MWS and HFSS may be appreciated, most notably up to 37.5 GHz. As intended by the optimised setup, the results show that the performance of the antenna with BMs closely resembles the one without BMs, except for a small increase of S_{11} below 20 GHz.

Figure 5 shows coupling for the antennas in gap 6 via a metallic target with 200 mm × 260 mm (MWS), 101 mm × 71 mm (HFSS), and 1000 mm × 1000 mm (tests) positioned 250 mm from the antennas, without (left) and with BMs (right). Without BMs coupling has no relevant features, with $97\%^{3dB}_{-60dB}$, increasing (like the antenna gain) towards the higher frequencies. With BMs there is an overall increase of coupling due to the focusing effect of the BMs, yet $78\%^{3dB}_{-60dB}$. The effect of

2020 JINST 15 C01033

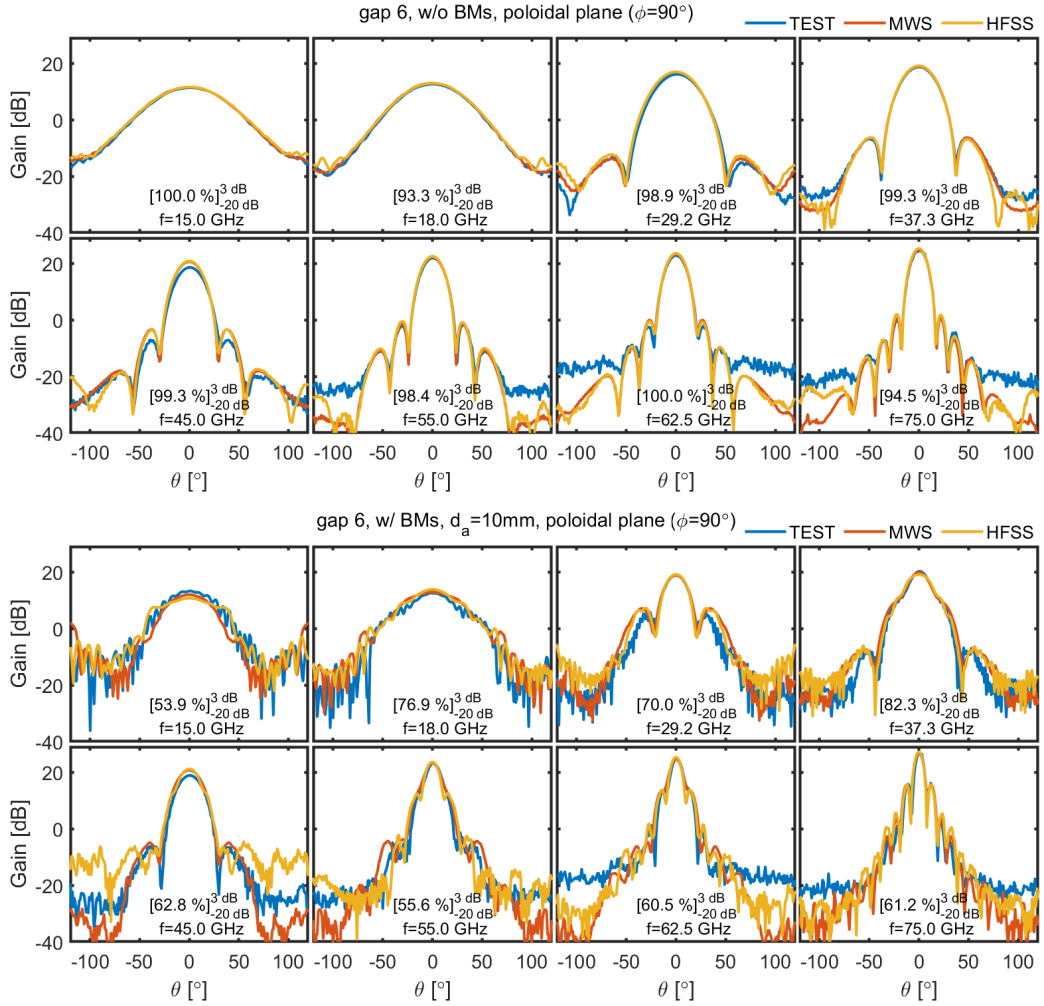

Figure 3. Radiation patterns for the antennas of gap 6 in the poloidal plane ($\phi = 90°$), simulated with HFSS and MWS and measured in the anechoic chamber tests, without BMs (top) and with BMs (bottom). Here, only the results with the antennas at $d_a = 10$ mm from the FW cut-outs are shown.

the reflections in the cut-outs shows up in the relatively large fluctuations up to ~30 GHz. Without BMs the overall behaviour shown by the prototype tests is well captured by both MWS and HFSS. With BMs, the agreement is even better — the observed discrepancies have to do with the different BM geometries and mirror dimensions used in MWS, HFSS and the tests (cf. figures 1 and 2).

3 Benchmarking of gap 4 results

Figure 6 illustrates the radiation patterns in the poloidal plane ($\phi = 90°$) from MWS and HFSS without and with the BMs of gap 4, showing that the most visible effect of the BMs is the shattering of the main lobe into multiple lobes of similar level that create multiple lines-of-sight to the target, which may reduce the performance of the system. Once again, the agreement between MWS and HFSS is clear — as for $\phi = 0°$ (not shown), — with $A_C^B > 80\%^{3dB}_{-60dB}$ for all frequencies since for this gap the BM models used in HFSS and MWS were identical (cf. figure 3).

2020 JINST 15 C01033

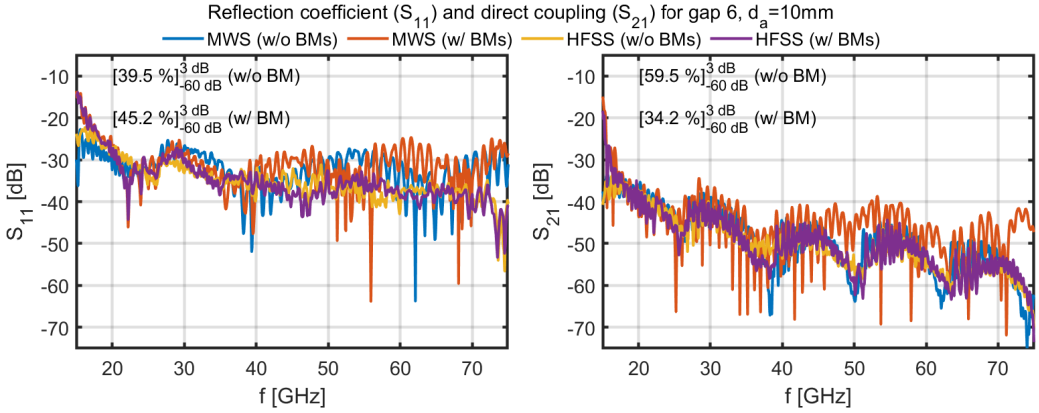

Figure 4. Reflection coefficient (S_{11}) and direct coupling (S_{21}) for gap 6 from HFSS and MWS, without and with BMs (d_a = 10 mm).

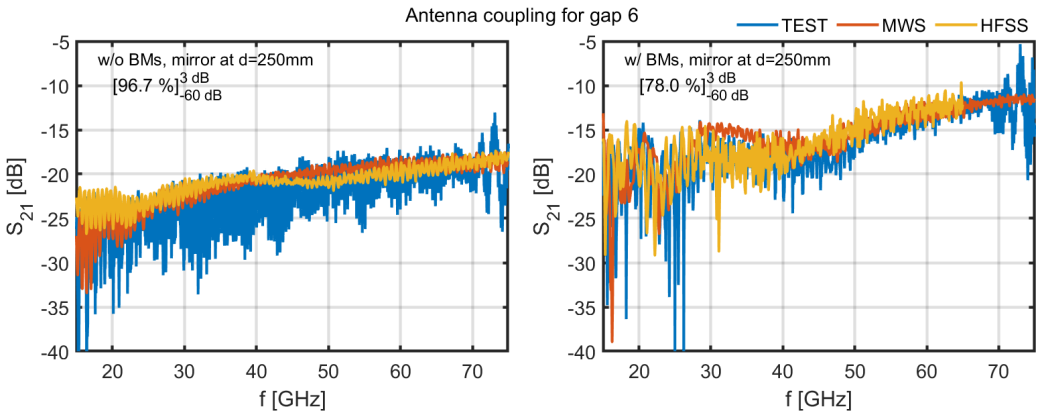

Figure 5. Antenna coupling with the target (at d = 250 mm) for gap 6 from HFSS, MWS and tests, without (left) and with BMs (right).

Figure 7 depicts coupling for the antennas in gap 4, direct (left) and via a target (right) [200 mm × 150 mm (HFSS) and 1000 mm × 1000 mm (tests)] at 250 mm from the antennas, where the accord between the HFSS and MWS estimations and between HFSS and the prototype tests can be assessed. Note that in the right figure A_C^B refers to the difference between HFSS and the test results. Although some fluctuations can be observed below ~25 GHz, these are not as pronounced as in gap 6. Above this frequency, there are no significant features induced by the presence of the BMs — reduction of coupling in the measurements at the higher frequencies is due to the cut-off (at 73.3 GHz) of a connector used. These results show that the BMs of gap 4 have less impact in the performance of the antennas, when compared to the ones of gap 6.

4 Conclusions

The studies show not only an overall agreement between HFSS and MWS but also an accord with the results obtained with the prototype tests, justifying the simplifications introduced in the models and revealing the important role of the EM simulations in optimising the antenna setup and in

2020 JINST 15 C01033

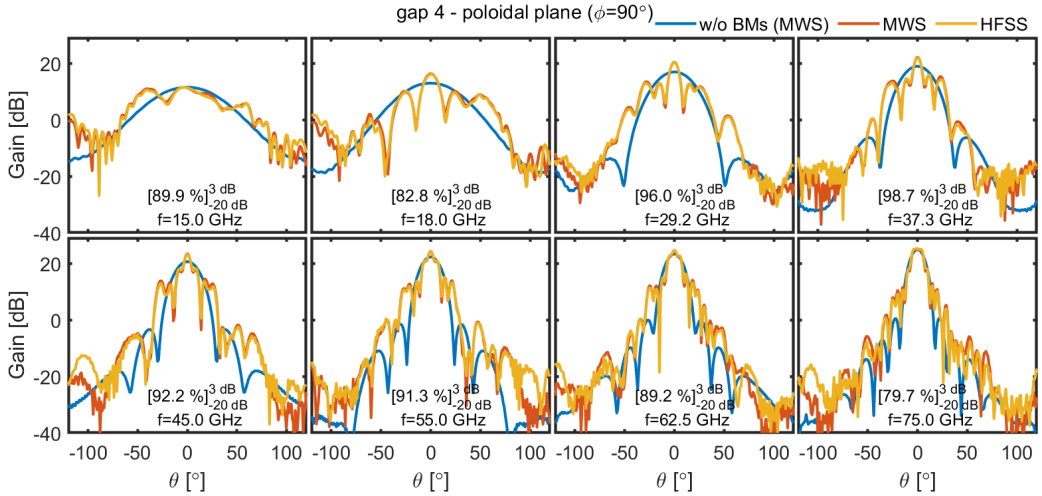

Figure 6. Radiation patterns for the antennas in gap 4 ($\phi = 90°$) simulated with HFSS and MWS. The results obtained without BMs from MWS are also shown for comparison.

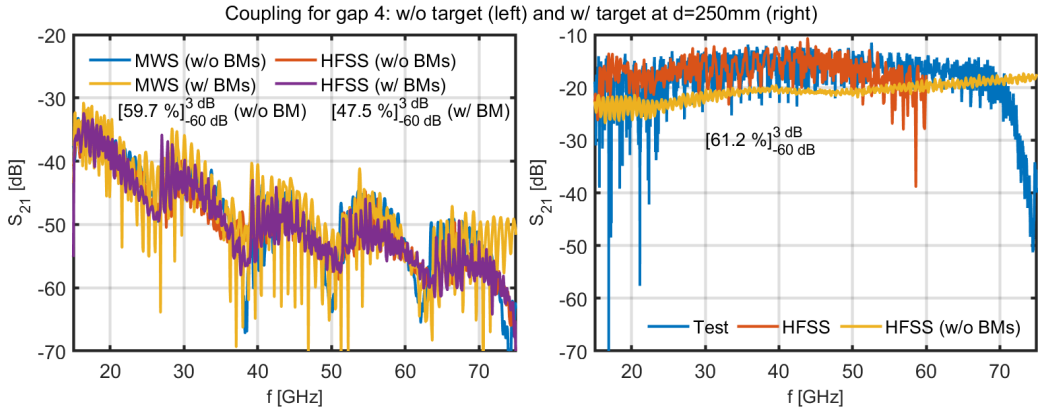

Figure 7. Left: direct coupling for the antennas in gap 4 from HFSS and MWS without and with BMs. Right: coupling via the metallic target from HFSS and tests — the HFSS result without BMs is also shown for comparison.

predicting the EM performance of gaps 4 and 6 before the prototyping phase. In particular, the simulations anticipated with precision the impact of the BMs and FW panels of each gap in the radiation patterns of the antennas and that moving the antennas towards the FW cut-outs of gap 6 could successfully mitigate their impact in the measurements.

Acknowledgments

The work leading to this publication has been funded partially by Fusion for Energy under the Specific Grant Agreement. IST activities also received financial support from Fundação para a Ciência e Tecnologia through project UID/FIS/50010/2019. This publication reflects the views only of the authors, and Fusion for Energy cannot be held responsible for any use which may be made of the information contained therein.

2020 JINST 15 C01033

References

[1] G. Vayakis et al., *Status and prospects for mm-wave reflectometry in ITER*, *Nucl. Fusion* **46** (2006) S836.

[2] P. Varela, J.H. Belo and P.B. Quental, *Performance assessment of the antenna setup for the ITER plasma position reflectometry in-vessel systems*, *Rev. Sci. Instrum.* **87** (2016) 11E713.

[3] P. Varela et al., *Report on the tests of the gap* 6 *antenna assembly prototype*, ITER report WWET5D, (2018).

2020 JINST 15 C01033